UCLA
UCLA Electronic Theses and Dissertations

Title
Compressive Wideband Spectrum Sensing based on Cyclostationary Detection

Permalink
https://escholarship.org/uc/item/7cc3918q

Author
Jain, Varun

Publication Date
2012

Peer reviewed|Thesis/dissertation

eScholarship.org Powered by the California Digital Library
University of California

University of California
Los Angeles

Compressive Wideband Spectrum Sensing based on Cyclostationary Detection

A thesis submitted in partial satisfaction
of the requirements for the degree
Master of Science in Electrical Engineering

by

Varun Jain

2012

Abstract of the Thesis

Compressive Wideband Spectrum Sensing based on Cyclostationary Detection

by

Varun Jain

Master of Science in Electrical Engineering

University of California, Los Angeles, 2012

Professor Danijela Cabric, Chair

Efficient use of the under-utilized spectrum is primarily dependent upon the accuracy of spectrum sensing in Cognitive Radios(CRs). To this end, wideband spectrum sensing is highly desirable as it increases the probability of detecting unused spectrum but it comes with a challenge of designing very high-speed A/D converters. Further, to achieve high throughput in CRs, primary users(PUs) must be detected within a constrained sensing time and under energy limitations. Here, we develop a reduced complexity compressive sampling cyclostationary detection method which exploits the two dimensional sparsity of the spectral correlation function (SCF). Detection is performed on the reconstructed Nyquist SCF which is obtained directly from the sub-Nyquist samples using a closed-form solution. For a given SCF sparsity, we quantify the bounds on the minmum lossless sampling rates which result in a unique reconstruction. Due to the additional sparsity introduced in the SCF with respect to the power spectral density, the minimum sampling rates for cyclostationary detection are shown to be lower than those required for energy detection.

The thesis of Varun Jain is approved.

Gregory J. Pottie

Babak Daneshrad

Danijela Cabric, Committee Chair

University of California, Los Angeles

2012

Table of Contents

1 Introduction 1

2 System Model and Problem Formulation 3

2.1 System Model 3

2.2 Spectral Correlation Function Overview 4

2.3 Discrete-Time Non-Asymptotic SCF and Two Dimensional Sparsity . . . 5

2.4 Signal Detection Using Nyquist SCF 6

2.5 Compressive Sampling to Obtain sub-Nyquist Samples 7

2.6 Objectives and Contributions 8

3 Nyquist-SCF Reconstruction using sub-Nyquist Samples 9

3.1 Relating Nyquist and Sub-Nyquist SCF 9

3.2 Restricted Isometry Property of the Measurement Matrix $\tilde{\mathbf{\Phi}}$ 11

3.3 Reconstruction of the Nyquist SCF 12

4 Measures for Uniqueness of the Reconstructed SCF 15

4.1 Spark of the Sensing Matrix $\tilde{\mathbf{\Phi}}$ 16

4.2 Probabilistic Spark of the Sampling Matrix 17

4.3 Condition for Uniqueness of the Reconstructed Nyquist SCF $\hat{\mathbf{s}}_x$ 20

5 Minimum Lossless Sampling Rates and Channel Sparsity 20

6 Discussion And Numerical Results 22

6.1 SCF Reconstruction Using the Proposed Algorithm 23

6.2 Theoretical Minimum Lossless Compression 24

6.3 Mean Squared Error (MSE) of the Reconstructed SCF 25

6.4 Sensing Time Requirements and Comparison to Nyquist Detection 26

6.5 Detection Performance of the Proposed Detector 28

7 A Practical Example: Modulated Wideband Converter (MWC) 31
7.1 System Overview 31
7.2 Recovery of Nyquist Samples 32
7.3 Numerical Results 33
8 Conclusion 34
References **35**

List of Figures

1 SCF Support for a Bandpass Signal. 7

2 Probability that every K_f columns of $\tilde{\mathbf{\Phi}}$ forms a full-column rank $\hat{\mathbf{\Phi}}$, where $Spark(\tilde{\mathbf{\Phi}}) \leq K_f \leq Rank(\tilde{\mathbf{\Phi}})$ for $M/N = 0.25$ and $M/N = 0.5$ for increasing values of N. 18

3 Probability that every K_f columns of $\tilde{\mathbf{\Phi}}$ forms a full-column rank $\hat{\mathbf{\Phi}}$, where $N \leq K_f \leq Rank(\tilde{\mathbf{\Phi}})$ for $M/N = 0.5$ for increasing vaues of N. The columns corresponding to PSD are always present in every subset. 19

4 Comparison of sub-Nyquist and Reconstructed SCFs at a compression ratio $M/N = 0.5$, L = 2000 averages and SNR = 0 dB. 23

5 Minimum Sampling rate vs PSD Sparsity 24

6 Minimum Squared Error(MSE) of Reconstructed Feature used for Signal Detection under Varying Sparsity Levels, $K = 1$ and $K = 3$ Signals. 26

7 Number of frames(L) required to reach $(P_{fa}, P_d) = (0.1, 0.9)$ versus SNR for Nyquist and sub-Nyquist based detectors for a Compression Ratio of $M/N = 0.5$, with $K = 1$ and 3 Signals. 27

8 Sensing Time versus Compression Ratio to reach $(P_{fa}, P_d) = (0.1, 0.9)$ for Varying Sparsity Levels, $K = 1$ and 3 Signals and SNR = -5 dB. 28

9 P_d versus P_{fa} for Varying Compression Ratio($\frac{M}{N}$) for $K = 3$ Signals, Number of Frame Averages L = 15000 and SNR = -10 dB. 29

10 P_d versus P_{fa} for Varying Frame Averages for $K = 3$ Signals, Compression Ratio M/N = 0.5 and SNR = -10 dB. 29

11 P_d versus P_{fa} for Varying SNR for $K = 3$ Signals, Compression Ratio M/N = 0.5 and Number of Frame Averages L = 15000. 30

12 P_d versus P_{fa} for different modulation classes at $L = 100$ frame averages and SNR = 0 dB. 33

List of Tables

1 Cyclic features for some modulation classes 5

Acknowledgments

One of the joys of completion is to look over the journey past and remember all the friends and family who have helped and supported me along this long but fulfilling road.

I would like to express my heartfelt gratitude to Professor Danijela Cabric, Professor Babak Daneshrad, Professor Greg. Pottie, and Professor Yonina C. Eldar who provided encouraging and constructive feedback. It is no easy task, reviewing a thesis, and I am grateful for their thoughtful and detailed comments.

My colleagues at the lab ensured I was constantly engaged and entertained along the way. In particular, I cant thank Eric Rebeiz's exceptional friendship enough. Among many other things, Eric gave me thoughtful and detailed feedback on this thesis, a careful and patient ear, and a gentle help in finding my balance. Paulo Isagani Urriza, Wesam Gabran, Jun Wang, Jason Tran and Deborah Cohen were insightful research partners who were also frank, warm, and open in their advice.

Above all, I would like to thank my family and friends who have given me their unequivocal support throughout, as always, for which my mere expression of thanks likewise does not suffice.

1 Introduction

It has been widely recognized that utilization of radio spectrum by licensed wireless systems, e.g., TV broadcasting is quite low. In particular, at any given time and spatial region, there are frequency bands where there is no signal occupancy. There has been growing interest in improving spectrum utilization by permitting secondary usage using Cognitive Radios(CRs). Cognitive radios use spectrum sensing to determine frequency bands that are vacant of primary users(PUs) and transmit on such portions to meet regulatory constraints of avoiding harmful interference to licensed systems. Conventional signal processing approaches for spectrum sensing assume detection of a narrowband signal in noise. Most commonly used techniques include matched filtering, energy detection, and cyclostationary detection [1–4]. The energy detection method is not robust against noise uncertiainty and fails to diffrentialte among signals. Other methods, such as matched filtering and preamble detection, require strong prior knowledge about the primary user. Although performing well under low SNR scenarios, these methods are not general enough, because each system eventually requires a matched filter specifically designed for it. In this thesis, we explore wideband spectrum sensing using cyclostationary feature detection [5] which relies on the detection of embedded cyclostationary features of modulated signals. This approach is robust against noise uncertainty since it exploits the stationary property of the noise process and hence asymptotically separates signal from noise, In addition, feature detectors are able to differentiate among signals with different modulation types.

Wideband spectrum sensing is highly desirable since sensing multiple channels simultaneously increases the probability of finding unused spectrum. But operating in a wideband regime faces considerable technical challenges as well. The radio front-end can employ a bank of tunable narrowband bandpass filters to search one narrow frequency band at a time. This requires an unfavorably large number of RF components and the tuning range of each filter is preset. Alternatively, a wideband circuit utilizes a single RF chain followed by high-speed DSP to flexibly search over multiple frequency bands concurrently [6]. A major implementation challenge lies in the very high sampling rates and dynamic range required by the A/D converters in such a scenario.

In order to reduce sampling rate requirements, Compressive sampling (CS) can be used as a method of acquisition and reconstruction of sparse signals [7]. Recently proposed compressive sensing analog front-end architectures include Analog to Information Converters (AIC) [8], Modulated Wideband Converters (MWC) [9–11], and other parallel mixed-signal architectures [12–14]. By exploiting the fact that the spectrum is under-utilized and therefore sparse, we can reconstruct the original wideband spectrum from the compressed signal using well-known approaches like Orthogonal Matching Pursuit (OMP) and the ESPRIT algorithm [15] which have high complexity. Further, reconstruction methods such as the ones in [16, 17] rely on numerical methods to solve an optimization problem, which make them difficult to implement in VLSI.

In this thesis, we consider a wideband compressive sampling based cyclostationary detector that exploits the two dimensional sparsity in the cyclic and angular frequency domains of the Spectral Correlation Function(SCF). The sparsity in the cyclic domain comes from the fact that features of modulated signals result in a few distinct peaks in the cyclic frequency domain while noise does not exhibit any spectral correlation peaks asymptotically. In order to detect the peaks of a PU signal, feature detectors first estimate the SCF [18]. The SCF can be reconstructed by first reconstructing the Nyquist samples from sub-Nyquist samples and then performing feature detection. Such an approach is presented in [19] using the MWC as a front-end. Conventional detectors include single-cycle and multi-cycle detectors which collect the energy in the SCF at one or many cyclic frequencies, respectively. Another approach is to reconstruct the SCF directly from the sub-Nyquist samples as was considered first in [20]. Here, the SCF reconstruction is performed blindly with no *a priori* knowledge of the carriers and bandwidths of the signals to be detected, and detection is performed on a per-band basis using a GLRT statistic.

In this work, we exploit the fact that in a typical CR setting, the sensing radios have some information about the signals to be detected. In other words, the goal of the CRs is to detect the presence or absence of one or many PUs simultaneously in a wideband channel, with *a priori* knowledge of their carrier frequencies, symbol rates, and modulation schemes. Similar to our previous work in [21], we explore a reduced complexity approach for reconstructing the Nyquist SCF from sub-Nyquist samples by formulating an optimization problem that exploits the knowledge about carrier frequencies and signal bandwidths of the signals to be detected.

The proposed algorithm reconstructs only useful spectral correlation peaks used for detection, resulting in a closed form solution to the optimization problem, making it energy efficient and implementable in VLSI. In addition, we theoretically analyze the minimum lossless compression ratios under a given SCF sparsity that guarantee a unique solution to the reconstruction problem. This presents a design guideline in terms of the achievable sampling rate reductions. We show that the proposed detector requires additional sensing time in order to improve detection performance up to a threshold compression point which we call the *Compression Wall*, below which the gains are negligible with increasing sensing time.

The rest of the thesis is organized as follows. In Section 2, we present our system model, give a brief overview on cyclostationary-based detection and the problem statement. In Section 3, we relate the SCF of the sub-Nyquist samples to the one using Nyquist samples, and formulate our reduced complexity optimization problem for reconstruction of the spectral peaks of interest. In Section 4 we derive the conditions necessary to guarantee a unique solution to the optimization problem. Section 6 gives the numerical results with a detailed discussion on the same. Finally, Section 8 concludes this thesis.

2 System Model and Problem Formulation

2.1 System Model

We consider a wideband channel with a total bandwidth of B Hz which is divided into a set non-overlapping narrowband subchannels. The bandwidth of each of the narrowband channel is not necessarily equal. We assume that K primary users, $s_k(t)$ $\forall k \in [1, ..., K]$, share this spectrum. However, depending on the location and time, some of these subchannels might not be used by primary users and are available for secondary transmission. We are interested in jointly indentifying these underutilized subbands. Given the time and energy constraints on the sensing stage, we consider a limited time window of length $T_{sense} = N_T T_s$ during which the sensing radio acquires a total number of N_T incoming samples, where T_s is the sampling period. For modeling the detection problem on each subchannel k, binary hypothesis testing is

used in which hypothesis $\mathcal{H}_{k,0}$ represents the absence of the primary signal and hypothesis $\mathcal{H}_{k,1}$ represents the presence of the primary signal. Therefore, the received wideband signal is given by

$$x(t) = \sum_{k=1}^{K} s_k(t) \ , \quad \text{where } 0 \leq t \leq T_{sense} \ \text{ and}$$

$$s_k(t) = \begin{cases} w_k(t) & \text{under } \mathcal{H}_{k,0} \\ \sum_{n=-\infty}^{\infty} \Re\{a_k(nT_k)p_k(t-nT_k)e^{j2\pi f_{c_k}t}\} + w_k(t), & \text{under } \mathcal{H}_{k,1}, \end{cases} \tag{1}$$

where $t \in [0, T_{sense})$ denotes the time variable, $a_k(nT)$ and $p_k(t)$ are the transmitted information symbols and the pulse shaping filter of the kth transmitted signal respectively, and $w_k(t)$ is the AWGN in the band occupied by the kth transmitter. We assume transmitted information symbols with average power $\sigma^2_{a_k}$, a pulse shape filter $p_k(t)$ of unit energy, and we define the Signal to Noise Ratio by SNR $= \sigma^2_{a_k}/\sigma^2_{w_k}$ where $\sigma^2_{w_k}$ is the noise variance in the channel occupied by $s_k(t)$.

For the analysis that follows, we assume perfect knowledge of the carrier frequencies f_{c_k}, symbol rates $1/T_k$ and the modulation scheme of the PUs that might be active in the wideband channel.

2.2 Spectral Correlation Function Overview

A random process $x(t)$ is said to be cyclostationary with a fundamental period T in the wide sense if its mean $E[x(t)] = \mu_x(t)$ and autocorrelation $E[x(t)x(t+\tau)] = R_x(t,\tau)$ are both periodic with a period T [5]. In the context of digital communications, T coincides with the symbol period of the modulation scheme.

$$E[x(t+T)] = \mu_x(t), \ \text{and} \ \ R_x(t+T,\tau) = R_x(t,\tau)$$

Now given a cyclostationary random process, its autocorrelation $R_x(t,\tau)$ can be expanded using the Fourier series as follows

$$R_x(t,\tau) = \sum_{\alpha} R_x^{\alpha}(\tau)e^{j2\pi\alpha t}$$

Table 1: Cyclic features for some modulation classes

Modulation	Peaks at (α, f)
BPSK	$(\frac{1}{T}, f_c)$, $(2f_c, 0)$, $(2f_c \pm \frac{1}{T}, 0)$
MSK	$(\frac{1}{T}, f_c)$, $(2f_c \pm \frac{1}{2T}, 0)$
QAM	$(\frac{1}{T}, f_c)$

where $\alpha = \ell/T$ for $\ell \in \mathbb{Z}$. In the equation above, $R_x^\alpha(\tau)$ are the Fourier series coefficients which can be expressed as

$$R_x^\alpha(\tau) = \frac{1}{T} \int_{-\infty}^{\infty} R_x(t, \tau) e^{-j2\pi\alpha t} \, \mathrm{d}t$$

Because of the nature of periodic signals, the Fourier Series of $R_x^\alpha(\tau)$ will have spectral peaks at $\alpha = \ell/T, \forall \ell \in \mathbb{Z}$. The asymptotic SCF is obtained by taking the Fourier Transform of $R_x^\alpha(\tau)$ with respect to τ, yielding $S_x(\alpha, f)$, namely

$$S_x(\alpha, f) = \int_{-\infty}^{\infty} R_x^\alpha(\tau) e^{-j2\pi f\tau} \, \mathrm{d}\tau$$

where α is referred to as the cyclic frequency, and f is the angular frequency. The α locations of the spectral correlation peaks of the SCF are solely a function of the modulation class being transmitted, the symbol rate $1/T$, and the carrier frequency f_c, all of which we assume to be known *a priori*. Note that AWGN is a widesense stationary process and exhibits no cyclic correlation. Therefore, the SCF of noise asymptotically has no spectral features at $\alpha \neq 0$.

The (α, f) locations of the spectral peaks of the SCF as a function of the modulation scheme are summarized in Table 1 for a few common modulation classes.

2.3 Discrete-Time Non-Asymptotic SCF and Two Dimensional Sparsity

Given the received wideband signal from (1), we get a frame of Nyquist samples $\mathbf{x} \in \mathbb{R}^N$ by sampling $x(t)$ at the Nyquist rate f_s. Hence, over the sensing period T_{sense}, we get N_T/N different frames of samples which are used for statistical averaging of the autocorrelation function of the signal. As we consider only a finite number of samples to obtain the autocorrelation matrix, perfect construction of the SCF is not possible. Therefore, the non-asymptotic Nyquist SCF is

computed as follows

$$\tilde{\mathbf{S}}_x = \mathbf{F}_N \left(\frac{N}{N_T} \sum_{\ell=1}^{N_T/N} \mathbf{x}_\ell \mathbf{x}_\ell^T \right) \mathbf{F}_N, \tag{2}$$

where N_T/N is the number of spectral averages, $\mathbf{x}_\ell$ is the ℓth data frame received, and $\mathbf{F}_N$ is a $N \times N$ DFT matrix. The frame length N determines the SCF resolution in both angular and cyclic frequency (being $1/NT_s$). Note that as the number of averages $N_T/N \to \infty$, the noise fluctuations are smoothened out and the estimated discrete SCF approaches the asymptotic continuous SCF [5]. Fig. 1 shows the support of the SCF for a real bandlimited signal which is a sparse two-dimensional spectral map with non-zero features at the cyclic / angular frequency pairs shown in Table 1 for different modulation classes and in the PSD corresponding to $\alpha = 0$. Thus, if we consider a sparse multiband signal $x(t)$ in (1), the noise being independent of the signal, the SCF of signal and SCF of noise are directly summed and the resultant SCF is sparse in both α and f.

2.4 Signal Detection Using Nyquist SCF

The presence/absence of one or multiple signals in the band of interest is detected by collecting energies in the non-zero points of the Nyquist SCF $\tilde{\mathbf{S}}_x$ in (2). In this thesis, we concentrate on a single-cycle detector which detects the energy of the most dominant peak present in the SCF, for e.g. the peak at $(2f_c, 0)$ for BPSK modulation. The noise in the wideband channel is assumed to be AWGN. Also, since cyclostationary detection is robust to interference from strong adjacent band signals, the received power from all the transmitters is assumed to be equal, yielding the same in-band SNR for all signals. Therefore, the detection performance across the bands of interest will be the same for all K signals and we drop the index k in the two hypotheses $\mathcal{H}_0$ and $\mathcal{H}_1$ in (1). The test statistic used for detection is given by

$$\mathcal{T} = |\tilde{\mathbf{S}}_x(\alpha, f)|^2 \tag{3}$$

where (α, f) corresponds to the $(2f_c, 0)$ peak in the Nyquist SCF. This statistic $\mathcal{T}$ is then compared to a threshold γ which is set according to an acceptable probability of false alarm in the system. The objective of the Nyquist-based detector is to meet a desired probability of false

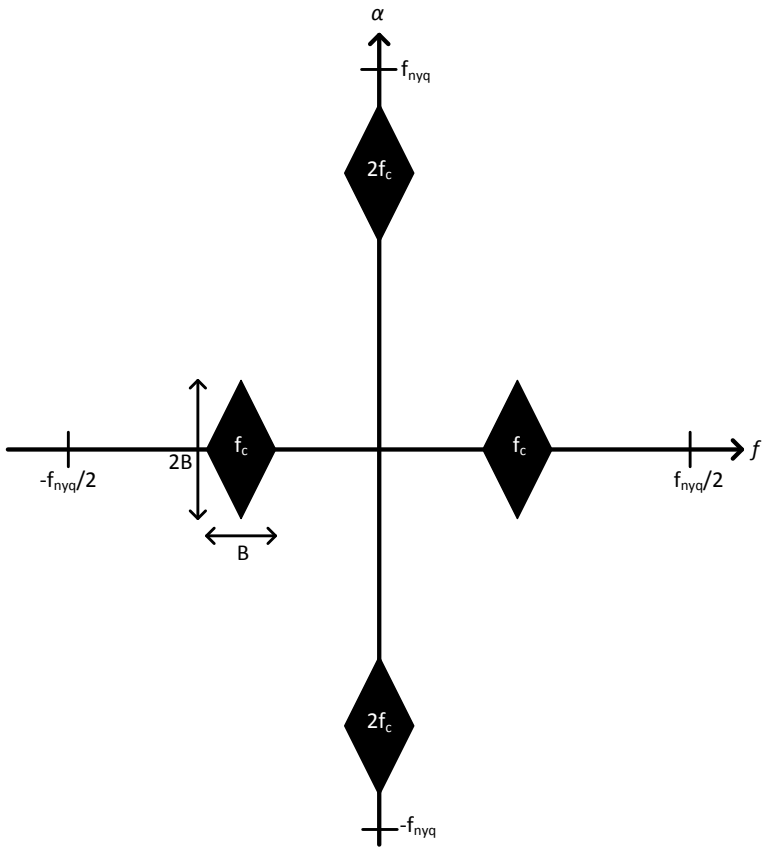

Figure 1: SCF Support for a Bandpass Signal.

alarm and probability of detection point on the receiver operating curve (ROC) curve, defined as $P_{fa} = \mathbb{P}(\mathcal{T} > \gamma|\mathcal{H}_0),\ P_d = \mathbb{P}(\mathcal{T} > \gamma|\mathcal{H}_1)$ respectively.

2.5 Compressive Sampling to Obtain sub-Nyquist Samples

As is shown in Fig. 1, the Nyquist SCF is a two dimensional spectral map of the signal which is sparse in α and f. Hence, based on compressive sensing theory [7], we can sample below the Nyquist rate and perform spectrum sensing on the sub-Nyquist samples. This reduces the high sampling rate requirements on the A/D converters making it possible to use the current day state-of-the-art data converters. In this thesis, the analog front-end used for sub-Nyquist sampling is modeled by a sampling matrix $\mathbf{A}$ which is assumed to be an i.i.d Gaussian matrix. Note that

for practical implementation of the compressive sensing algorithms, sub-Nyquist samples can be obtained directly from any of the analog front-ends [8, 13, 14].

For a fixed T_{sense}, instead of acquiring N_T samples at a high rate f_s, we acquire M_T samples at a rate $\frac{M_T}{N_T} f_s \leq f_s$. The M_T samples will result in M_T/M different frames to be processed for detection where we let $\mathbf{z} \in \mathbb{R}^M$ denote a frame of sub-Nyquist samples. Thus, a single frame of sub-Nyquist samples $\mathbf{z}$ is related to the frame of Nyquist samples $\mathbf{x}$ via $\mathbf{z} = Ax$, where $\mathbf{A} \in \mathbb{R}^{M \times N}$ is the sampling matrix. As a result of the matrix multiplication, the *Compression Ratio* is defined as $\frac{M}{N}$. Using the sub-Nyquist samples, the Nyquist SCF is reconstructed by solving a standard least-squares problem, using which the signal detection is performed.

2.6 Objectives and Contributions

In compressive sensing, ℓ_1 minimization algorithms often use linear programming or other optimization methods to recover the sparse signal vectors. Such algorithms are often very demanding in computational complexity for applications involving very large problem dimensions and are difficult to implement in VLSI. But, given the *a priori* knowledge about the signal parameters, namely the modulation class, the carrier frequency, and the symbol rate of the PU that we wish to detect, we explore a reduced complexity solution to the SCF reconstruction and express the solution of the optimization problem in closed-form.

We derive the conditions needed to guarantee uniqueness of the reconstructed SCF and also investigate probabilistic measures of its applicability. Based on these conditions, we quantify the minimum lossless sampling rates acheivable for feature-based and energy-based detectors.

Finally, we propose a cyclostationary detection method based on sub-Nyquist samples which exploits the two dimensional sparsity in the Nyquist SCF and understand the tradeoffs between compression, sensing time, and the resulting detection performance.

3 Nyquist-SCF Reconstruction using sub-Nyquist Samples

In this section, we propose an algorithm to reconstruct the Nyquist SCF directly from sub-Nyquist samples which are obtained using the sampling model $\mathbf{z} = \mathbf{A}\mathbf{x}$. We start by deriving an expression relating the Nyquist and sub-Nyquist SCF which is subsequently used to formulate an optimization problem for reconstruction. Given that we know the modulation scheme, carrier frequency and symbol rate of the transmitted signal, we only reconstruct specific points of the SCF, reducing the optimization to a regular least-squares problem which can be solved in closed-form. The reconstructed SCF is then used to detect the presence or absence of the primary user, comparing the energy of the SCF at the location of the most dominant peak of the signal to a threshold γ.

3.1 Relating Nyquist and Sub-Nyquist SCF

Given multiple measurement vectors $\mathbf{z}$ of sub-Nyquist samples, we start by defining its non-asymptotic autocorrelation matrix $\mathbf{R}_z \in \mathbb{R}^{M\times M}$ which is required to compute the SCF,

$$\mathbf{R}_z = \frac{1}{L}\sum_{\ell=1}^{L} \mathbf{z}_\ell \mathbf{z}_\ell^T \tag{4}$$

where $L = M_T/M$ frames of $\mathbf{z}$ are considered for statistical averaging and $\mathbf{z}_l \in \mathbb{R}^M$ is a frame of sub-Nyquist samples. Given our sampling model, $\mathbf{z} = \mathbf{A}\mathbf{x}$, it follows that the Nyquist autocorrelation matrix $\mathbf{R}_x \in \mathbb{R}^{N\times N}$ and $\mathbf{R}_z$ are related via

$$\mathbf{R}_z \;=\; \mathbf{A}\mathbf{R}_x\mathbf{A}^T$$

Vectorizing both sides of the equation gives the following

$$\mathbf{r}_z \;=\; (\mathbf{A}\otimes\mathbf{A})\mathbf{r}_x \triangleq \mathbf{\Phi}\mathbf{r}_x \tag{5}$$

where $\otimes$ is the Kronecker product, $\mathbf{r}_x = \mathrm{vec}(\mathbf{R}_x)$, $\mathbf{r}_z = \mathrm{vec}(\mathbf{R}_z)$ and $\mathbf{\Phi} = \mathbf{A}\otimes\mathbf{A} \in \mathbb{C}^{M^2\times N^2}$.

The SCF matrix $\mathbf{S}_x$ is obtained by taking Fourier transform of $\mathbf{R}_x$ with respect to its columns on the right and rows on the left. This is expressed as

$$\mathbf{S}_x \;=\; \mathbf{F}_N\mathbf{R}_x\mathbf{F}_N^H$$

where $\mathbf{F}_N$ is a $N \times N$ DFT matrix. Again performing the vec operation on this equation gives

$$\mathbf{s}_x = \mathbf{T}_x \mathbf{r}_x \tag{6}$$

where $\mathbf{s}_x = \text{vec}(\mathbf{S}_x)$ and $\mathbf{T}_x = \mathbf{F}_N \otimes \mathbf{F}_N \in \mathbb{C}^{N^2 \times N^2}$. The matrix $\mathbf{T}_x$ consists of two N-point DFT matrices $\mathbf{F}_N$ which are responsible for the transformation of the (t, τ) time-domain pair of $\mathbf{r}_x$ to the (α, f) pair in the SCF. Similarly, we obtain $\mathbf{s}_z = \mathbf{T}_z \mathbf{r}_z$ where $\mathbf{s}_z = \text{vec}(\mathbf{S}_z)$, $\mathbf{T}_z = \mathbf{F}_M \otimes \mathbf{F}_M \in \mathbb{C}^{M^2 \times M^2}$ and $\mathbf{F}_M$ is a M-point DFT matrix.

$\mathbf{T}_x$ and $\mathbf{T}_z$ are square invertible matrices since they are composed of DFT matrices which are also square and invertible and $Rank(\mathbf{A} \otimes \mathbf{B}) = Rank(\mathbf{A})Rank(\mathbf{B})$. Hence, $\mathbf{T}_x^\dagger \mathbf{T}_x = \mathbf{T}_x \mathbf{T}_x^\dagger = \mathbf{I}_{N^2 \text{x} N^2}$ where $\dagger$ denotes the pseudo-inverse operation. Also, $\mathbf{T}_x$ and $\mathbf{T}_z$ are orthogonal matrices since they are formed using DFT matrices. This can be seen as follows

$$\begin{aligned}(\mathbf{F}_N \otimes \mathbf{F}_N)^T (\mathbf{F}_N \otimes \mathbf{F}_N) &= (\mathbf{F}_N^T \otimes \mathbf{F}_N^T)(\mathbf{F}_N \otimes \mathbf{F}_N) \\ &= (\mathbf{F}_N^T \mathbf{F}_N \otimes \mathbf{F}_N^T \mathbf{F}_N) = \mathbf{I}_N \otimes \mathbf{I}_N = \mathbf{I}_{N^2}\end{aligned}$$

Now, as $\mathbf{T}_x$ is an orthogonal matrix, $\mathbf{T}_x^H = \mathbf{T}_x^\dagger$ and hence $\mathbf{T}_x^H \mathbf{T}_x = \mathbf{T}_x \mathbf{T}_x^H = \mathbf{I}_{N^2 \text{x} N^2}$. We now relate $\mathbf{s}_x$ and $\mathbf{s}_z$ using equation (5) as follows

$$\begin{aligned}\mathbf{T}_z \mathbf{r}_z &= \mathbf{T}_z \mathbf{\Phi} \mathbf{r}_x \\ \mathbf{s}_z = \mathbf{T}_z \mathbf{\Phi} \mathbf{r}_x &= \mathbf{T}_z \mathbf{\Phi} \mathbf{T}_x^H \mathbf{T}_x \mathbf{r}_x \triangleq \tilde{\mathbf{\Phi}} \mathbf{s}_x,\end{aligned} \tag{7}$$

where $\tilde{\mathbf{\Phi}} = \mathbf{T}_z \mathbf{\Phi} \mathbf{T}_x^H \in \mathbb{C}^{M^2 \text{x} N^2}$. The equation above relates the vectorized SCF of the sub-Nyquist samples to that of the Nyquist samples via the measurement matrix $\tilde{\mathbf{\Phi}}$. In order to ensure stable reconstruction of $\mathbf{s}_x$, $\tilde{\mathbf{\Phi}}$ must satisfy the Restricted Isometry Property (RIP) as has been shown by [7], [22]. In the next section, we show that the way we construct $\tilde{\mathbf{\Phi}}$ in our algorithm guarantees that it will satisfy RIP with high probability.

3.2 Restricted Isometry Property of the Measurement Matrix $\tilde{\mathbf{\Phi}}$

Using equation (7), we see that the measurement matrix $\tilde{\mathbf{\Phi}}$ is composed of i.i.d Gaussian matrix and DFT matrices. $\tilde{\mathbf{\Phi}}$ can be expanded as

$$\begin{aligned}
\tilde{\mathbf{\Phi}} &= \mathbf{T}_z \mathbf{\Phi} \mathbf{T}_x^H \\
&= (\mathbf{F}_M \otimes \mathbf{F}_M)(\mathbf{A} \otimes \mathbf{A})(\mathbf{F}_N \otimes \mathbf{F}_N)^H \\
&= (\mathbf{F}_M \otimes \mathbf{F}_M)(\mathbf{A} \otimes \mathbf{A})\left(\mathbf{F}_N^H \otimes \mathbf{F}_N^H\right) \\
&= \left(\mathbf{F}_M \mathbf{A} \mathbf{F}_N^H\right) \otimes \left(\mathbf{F}_M \mathbf{A} \mathbf{F}_N^H\right) \qquad (8)
\end{aligned}$$

where the last two equalities come from the properties of Kronecker product of matrices.

Previous works have shown that RIP holds with high probability for matrices whose entries are independent and identically distributed (i.i.d.) realizations of certain random distributions like the Gaussian distribution [23]. Hence, in order to prove that $\tilde{\mathbf{\Phi}}$ satisfies RIP, we start by showing that the elements of $\left(\mathbf{F}_M \mathbf{A} \mathbf{F}_N^H\right)$ are i.i.d Gaussian distributed using the following Lemma.

Lemma 1. *Let* $\mathbf{A}$ *be a* $M \times N$ *full row-rank matrix* ($M \leq N$) *whose elements are i.i.d with Gaussian distribution, and let* $\mathbf{B} \in \mathbb{C}^{N \times N}$ *and* $\mathbf{C} \in \mathbb{C}^{M \times M}$ *be unitary matrices. Then the elements of* $\mathbf{AB}$ *and* $\mathbf{CA}$ *are also i.i.d Gaussian distributed.*

Proof. We know that given two random variables x and y with distributions $f_x(x)$ and $f_y(y)$ respectively, their joint distribution $f_{xy}(xy) = f_x(x) f_y(y)$ iff x and y are independent random variables.

Given a i.i.d Gaussian distributed matrix $\mathbf{A}$, the joint element density is expressed as

$$\begin{aligned}
f(a_{11}, a_{12}, ..., a_{mn}) &= f(a_{11}) f(a_{12}) .... f(a_{mn}) \\
&= \frac{1}{(2\pi\sigma^2)^{\frac{mn}{2}}} \exp\left(-\frac{1}{2\sigma^2}({a_{11}}^2 + {a_{12}}^2 + ... + {a_{mn}}^2)\right) \\
&= \frac{1}{(2\pi\sigma^2)^{\frac{mn}{2}}} \exp\left(-\frac{1}{2\sigma^2}||\mathbf{A}||_F^2\right)
\end{aligned}$$

where $\mathbf{A}_{i,j} \sim (0, \sigma^2) \forall i, j$ and $||.||_F$ is the Frobenius norm. Now, using the fact that the Frobenius norm is invariant under unitary transformation, i.e. $||\mathbf{AB}||_F = ||\mathbf{CA}||_F = ||\mathbf{A}||_F$, it follows

directly from the joint element density of $\mathbf{A}$ that the elements of $\mathbf{AB}$ and $\mathbf{CA}$ are also i.i.d Gaussian distributed. $\square$

A direct result from the Lemma 1 is that the elements of $\mathbf{C}AB$ are also i.i.d Gaussian distributed. Hence, the elements of $\left(\mathbf{F}_M \mathbf{A} \mathbf{F}_N^H\right)$ are i.i.d Gaussian distributed as $\mathbf{F}_N$ and $\mathbf{F}_M$ are unitary matrices and $\mathbf{A}$ is i.i.d Gaussian distributed. From (8), the final step to prove that $\tilde{\mathbf{\Phi}}$ satisfies RIP is to study the RIP property of the Kronecker product of two i.i.d Gaussian matrices. From [24] we have,

$$\delta_K(\mathbf{\Psi}_1 \otimes \mathbf{\Psi}_2 \otimes .... \otimes \mathbf{\Psi}_D) \geq \max_{1 \leq d \leq D} \delta_K(\mathbf{\Psi}_d)$$

where $\delta_K(\mathbf{\Psi}_1), ..., \delta_K(\mathbf{\Psi}_D)$ are the restricted isometry constants of the matrices $\mathbf{\Psi}_1, ..., \mathbf{\Psi}_D$. Hence, $\delta_K(\mathbf{\Psi} \otimes \mathbf{\Psi}) \geq \delta_K(\mathbf{\Psi})$ where $\mathbf{\Psi}$ is an i.i.d Gaussian distributed matrix. Further, [25] gives an upper bound on the RIP constant of Kronecker product of matrices

$$\delta_K(\mathbf{\Psi}_1 \otimes \mathbf{\Psi}_2 \otimes .... \otimes \mathbf{\Psi}_D) \leq \prod_{d=1}^{D} (1 + \delta_K(\mathbf{\Psi}_d)) - 1$$

Hence, $\delta_K(\mathbf{\Psi} \otimes \mathbf{\Psi}) \leq \delta_K(\mathbf{\Psi})^2 + 2\delta_K(\mathbf{\Psi})$. As $\mathbf{\Psi}$ satisfies RIP with high probability with $0 < \delta_K(\mathbf{\Psi}) < 1$, thus $\delta_K(\mathbf{\Psi})^2$ is very small and $\delta_K(\mathbf{\Psi})^2 + 2\delta_K(\mathbf{\Psi}) < \delta_K(\mathbf{\Psi}) + 2\delta_K(\mathbf{\Psi}) = 3\delta_K(\mathbf{\Psi})$. Therefore, $\delta_K(\mathbf{\Psi} \otimes \mathbf{\Psi})$ is bounded as follows

$$\delta_K(\mathbf{\Psi}) \leq \delta_K(\mathbf{\Psi} \otimes \mathbf{\Psi}) \leq 3\delta_K(\mathbf{\Psi}) \tag{9}$$

The resulting pair of bounds is tight since $\delta_K(\mathbf{\Psi}) \ll 1$ and hence $3\delta_K(\mathbf{\Psi})$ is very small. This implies that the Kronecker product of two i.i.d Gaussian matrices, $(\mathbf{\Psi} \otimes \mathbf{\Psi})$, satisfies RIP with high probability. Hence, the measurement matrix $\tilde{\mathbf{\Phi}}$ satisfies the RIP with high probability as well.

3.3 Reconstruction of the Nyquist SCF

In the previous section we have shown that $\tilde{\mathbf{\Phi}}$, which relates $\mathbf{s}_x$ and $\mathbf{s}_z$ in (7), satisfies RIP with high probability which guarantees a stable reconstruction of the vectorized Nyquist SCF. Also, from Fig. 1, the SCF is sparse in both α and f and hence we can formulate the SCF

reconstruction as a standard least-squares problem by introducing an l_1 minimization term to account for the sparsity, namely

$$\min_{\mathbf{s}_x} ||\mathbf{s}_x||_1 + \lambda||\mathbf{s}_z - \tilde{\mathbf{\Phi}}\mathbf{s}_x||_2^2. \tag{10}$$

for some $\lambda > 0 \in \mathbb{R}$.

In order to detect signals in a wideband channel, we collect energies at the locations of the spectral correlation peaks in the reconstructed SCF. But, since the specral correlation peaks are discrete in the cyclic frequency domain α, the resolution required in the SCF for the spectral correlation peaks to be prominent is high. The resolution in both f and α is solely determined by the FFT size N, and is equal to f_s/N where f_s is the Nyquist sampling rate. Hence, a high resolution requirement translates into a large value of N. This leads to a high computational complexity in (10) since $\mathbf{s}_x$ is in $\mathbb{C}^{N^2}$. However, given that the sensing radios have *a priori* knowledge of the carrier frequencies, symbol rates, and modulation schemes of the licensed users, we know exactly the number and locations of the non-zero points of the SCF. Hence, we need to reconstruct only these K_f non-zero points in the SCF where $K_f \ll N^2$, making the reconstruction problem more computationally efficient.

We now derive an expression for K_f from the two-dimensional SCF given in Fig. 1. Here, each bandlimited signal k, for $k \in [1, ..., K]$, with bandwidth B_k occupies four lozenges with diagonals B_k and $2B_k$. Hence the total number of points K_f out of N^2 points of the SCF occupied by K signals is

$$K_f = 4K(\frac{B_k N}{f_s})^2 \tag{11}$$

where $(\frac{B_k N}{f_s})^2$ is the area of one of the four lozenges and K is the total number of signals present. The above expression for K_f assumes that we are operating in a high SNR regime($\geq$ 10dB). At low SNRs($<$ 10dB), as the noise power is high, the PSD is not sparse and we include points corresponding to the entire PSD in addition to those due to the signals.

$$K_f = 4K(\frac{B_k N}{f_s})^2 + N - 2K(\frac{B_k N}{f_s}) \tag{12}$$

where N accounts for N PSD points in the SCF and the factor $2K(\frac{B_k N}{f_s})$ accounts for the overlap between the total number of points occupied by K signals at high SNRs and the PSD. Note that

the expressions above assume that there are K_f non-zero elements in the Nyquist SCF when the number of averages L in (4) are sufficient to make the SCF sparse. When more spectral correlation peaks are prominent due to limited number of samples, K_f acts as a lower bound to the number of non-zero points in the SCF.

From (11) and (12), we observe that the number of features K_f is a function of the number of signals present in the wideband channel, their bandwidths, the resolution of the SCF (determined by N and the sampling rate) and the modulation class of the signals being detected (Table 1). Furthermore, it is evident that as long as the band of interest is not fully populated by signals, i.e. $K(\frac{B_k}{f_s})^2 \ll 1$, then the ratio of the number of features K_f to the total points in the SCF N^2 is very small or $K_f \ll N^2$. Therefore, we can reduce the dimensionality of the optimization problem in (10), decreasing the computational complexity of the reconstruction substantially.

The reduced dimensionality SCF is defined as

$$\hat{\mathbf{s}}_x = \mathbf{M}_f \mathbf{s}_x$$

where $\mathbf{M}_f \in \mathbb{R}^{K_f \times N^2}$ is a diagonal matrix with elements equal to 1 at the indices of possible cyclic features and $\hat{\mathbf{s}}_x \in \mathbb{C}^{K_f \times 1}$. Furthermore, we also define the matrix $\hat{\mathbf{\Phi}} = \tilde{\mathbf{\Phi}}_{\{j=1:K_f\}}$, which selects the corresponding K_f columns of $\tilde{\mathbf{\Phi}}$ and stores them in $\hat{\mathbf{\Phi}}$. Since we are only reconstructing the non-zero points in the SCF vector, we can therefore drop the ℓ_1 minimization term related to the SCF sparsity in (10), and the unconstrained optimization problem becomes

$$\min_{\hat{\mathbf{s}}_x} ||\mathbf{s}_z - \hat{\mathbf{\Phi}}\hat{\mathbf{s}}_x||_2^2 \tag{13}$$

which is an optimization in $\mathbb{C}^{K_f}$, where $K_f \ll N^2$. The reconstruction above is a regular least-squares problem which can be solved in closed form as follows

$$\hat{\mathbf{s}}_x = \hat{\mathbf{\Phi}}^{\dagger}\mathbf{s}_z \tag{14}$$

Hence, starting from (10), we have obtained a reduced complexity closed-form expression for the reconstruction of the Nyquist SCF without reconstructing the time doman Nyquist samples.

The solution to (14) is unique if the matrix $\hat{\mathbf{\Phi}}$ is full column rank. Since $\hat{\mathbf{\Phi}} = \tilde{\mathbf{\Phi}}_{\{j=1:K_f\}}$, in the next section we analyze the measurement matrix $\tilde{\mathbf{\Phi}}$ and derive the conditions which result

in a unique solution to the proposed reconstruction problem, a core requirement of compressive sensing algorithms.

4 Measures for Uniqueness of the Reconstructed SCF

A unqiue solution to the least-squares problem in (13) exists, if $\hat{\mathbf{\Phi}}$ is full column rank. The number and indices of the K_f columns of $\tilde{\mathbf{\Phi}}$ that comprise $\hat{\mathbf{\Phi}}$ are a function of the non-zero points in the SCF. Hence, we study the uniqueness conditions as a function of the cardinality of the vector $\mathbf{s}_x$, defined as

$$\mathcal{C}(\mathbf{s}_x) = ||\mathbf{s}_x||_0 \triangleq K_f. \tag{15}$$

where $\mathcal{C}(\mathbf{s}_x)$ is determined by the number of signals present in the wideband channel, and by their bandwidths.

To study the uniqueness of the reconstructed vector we start by finding the *Rank* of the measurement matrix $\tilde{\mathbf{\Phi}} = \mathbf{T}_z \mathbf{\Phi} \mathbf{T}_x^H$. From the *Rank* property of Kronecker product of matrices we have, $Rank(\mathbf{T}_z) = M^2$ since $Rank(\mathbf{F}_M \otimes \mathbf{F}_M) = Rank(\mathbf{F}_M)Rank(\mathbf{F}_M)$. Similarly, $Rank(\mathbf{\Phi}) = M^2$ and $Rank(\mathbf{T}_x^H) = N^2$. Hence, $\tilde{\mathbf{\Phi}}$ is the product of three full-rank matrices and the $Rank(\tilde{\mathbf{\Phi}})$ $= \min(M^2, M^2, N^2) = M^2$ since $M \leq N$. This proves that there cannot exist a set of more than M^2 columns of $\tilde{\mathbf{\Phi}}$ that are linearly independent. However, this does not mean that every set of M^2 or lesser columns of $\tilde{\mathbf{\Phi}}$ are linearly independent. To guarantee a unique solution to the reconstruction problem, we need to ensure that every subset of K_f columns of $\tilde{\mathbf{\Phi}}$ are independent. For this reason, we use the *Spark* of a matrix which is defined as,

$$Spark(\mathbf{A}) = \min_{d} ||\mathbf{d}||_0 \ \text{ such that } \mathbf{Ad} = 0 \tag{16}$$

From the definition in (16), the *Spark* of a matrix is the smallest number s such that there exists a set of s columns in the matrix that are linearly dependent. In other words, every subset of $(Spark - 1)$ columns or lesser of a matrix will be independent with probability 1. It is straightforward to see that, $2 \leq Spark \leq Rank + 1$. The section below is aimed at finding the *Spark* of the matrix $\tilde{\mathbf{\Phi}}$.

4.1 Spark of the Sensing Matrix $\tilde{\mathbf{\Phi}}$

It was shown in [24] that if $\mathbf{A} \in \mathbb{R}^{M \times N}$ is a rank-deficient matrix, i.e. $Rank(A) < N$, then the $Spark(\mathbf{A} \otimes \mathbf{A}) = Spark(\mathbf{A})$. Therefore, using (8), in order to find $Spark(\tilde{\mathbf{\Phi}})$, it is sufficient to find $Spark(\mathbf{F}_M \mathbf{A} \mathbf{F}_N^H)$.

We start by finding the $Spark$ of the time-domain sampling matrix $A \in \mathbb{R}^{M \times N}$. For any proper subspace U, the projection $P_{U^\perp x}$ of a Gaussian random vector x onto the orthogonal complement of U is also Gaussian, and further $x \in U$ when $P_{U^\perp x} = 0$, which occurs with probability 0. Thus, the M Gaussian random vectors will be linearly independent with probability 1, and taking a union bound over the $\begin{pmatrix} N \\ M \end{pmatrix}$ submatrices gives that the entire Gaussian random matrix is full spark with $Spark(\mathbf{A}) = M + 1$.

In order to find the $Spark$ of $\mathbf{F}_M \mathbf{A}$, we use the following Lemma.

Lemma 2. *Let* $\mathbf{A}$ *be a* $N \times N$ *invertible matrix, and let* $\mathbf{B}$ *be a* $N \times M$ *rank deficient matrix. Then* $Spark(\mathbf{AB}) = Spark(\mathbf{B})$.

Proof. Using the definition of $Spark$,

$$Spark(\mathbf{AB}) = \min_{\mathbf{d}} ||\mathbf{d}||_0 \text{ such that } \mathbf{ABd} = \mathbf{0}.$$

Given that matrix $\mathbf{A}$ is invertible, the constraint is equivalent to $\mathbf{Bd} = \mathbf{0}$. Hence,

$$Spark(\mathbf{AB}) = \min_{\mathbf{d}} ||\mathbf{d}||_0 \text{ such that } \mathbf{Bd} = \mathbf{0}$$

which is the definition of $Spark(\mathbf{B})$. Therefore, $Spark(\mathbf{AB}) = Spark(\mathbf{B})$. □

Therefore, using Lemma 2, $Spark(\mathbf{F}_M \mathbf{A}) = M + 1$. Now from Lemma 1, we know the Gaussian distribution is invariant to unitary transformation. Hence, the elements of $(\mathbf{A}\mathbf{F}_N^H)$ are also i.i.d Gaussian distributed and thus $Spark(\mathbf{A}\mathbf{F}_N^H) = Spark(\mathbf{A}) = M + 1$.

The above results prove that $Spark(\mathbf{F}_M \mathbf{A} \mathbf{F}_N^H) = M + 1$. Hence, this proves that $Spark(\tilde{\mathbf{\Phi}}) = M + 1$ since $Spark(\mathbf{F}_M \mathbf{A} \mathbf{F}_N^H \otimes \mathbf{F}_M \mathbf{A} \mathbf{F}_N^H) = Spark(\mathbf{F}_M \mathbf{A} \mathbf{F}_N^H)$ [24]. Hence, we can guarantee that as long as $K_f < M + 1$, then the resulting $\hat{\mathbf{\Phi}}$ matrix will be full column rank and the reconstruction in (14) will have a unique solution. This proves the following theorem.

Theorem 1. *There exists a unique solution to the reconstruction problem* $\mathbf{s}_z = \hat{\mathbf{\Phi}}\hat{\mathbf{s}}_x$ *with probability 1, iff* $K_f = ||\mathbf{s}_x||_0 < Spark(\tilde{\mathbf{\Phi}}) = (M+1)$.

Theorem 1 guarantees the existence of a unique solution with probability 1 if the criteria $(M+1) > K_f$ is met. However, the uniqueness criteria can still be met with $(M+1) \leq K_f$ with a non-zero probability. In the section below, we show that a unique solution to the reconstruction problem can be obtained with a quite high probability even when $(M+1) \leq K_f$, which is a typical case in the problem of reconstruction of the Nyquist SCF.

4.2 Probabilistic Spark of the Sampling Matrix

As a result of the *Spark* of the matrix $\hat{\mathbf{\Phi}}$ from the previous section, we know that every subset of $K_f < (M+1)$ columns of $\hat{\mathbf{\Phi}}$ are independent giving a unique solution to (13). Given that $Rank(\hat{\mathbf{\Phi}}) = M^2$, we are interested in the case, $(M+1) \leq K_f \leq M^2$. In this regime, $\hat{\mathbf{\Phi}} = \tilde{\mathbf{\Phi}}_{\{j=1:K_f\}}$ will be full-column rank with a certain non-zero probability p_{K_f}. Unfortunately, the probability p_{K_f} is NP-hard to compute [26], since similar to the *Spark* of the matrix, it entails finding all possible subsets of K_f columns of $\tilde{\mathbf{\Phi}}$ that are independent. Therefore, the rest of this section is focused on finding the probability p_{K_f} empirically that will result in a unique solution to the reconstruction.

From the definition of the *Spark*, there is a non-zero probability that at least one subset of K_f columns is dependent when K_f is in the range $M+1 \leq K_f \leq M^2$. In order to calculate the probability p_{K_f}, we proceed by empirically finding the maximum number of independent sets of K_f columns in $\tilde{\mathbf{\Phi}}$. Fig. 2 shows the probabililty p_{K_f} that all possible subsets of K_f columns of $\tilde{\mathbf{\Phi}}$ are independent as a percentage of total columns N^2. We compare p_{K_f} for two compression ratios, $M/N = 0.25$ and 0.5. In addition, at each compression ratio, we vary M and N (resolution in the SCF) to see if there is any gain or loss in terms of p_{K_f}. From the curves in Fig.2, we can make three important observations.

Firstly, the probability p_{K_f} that all subsets of $M+1 \leq K_f \leq M^2$ columns will be independent is much higher at lower compression ratios ($M/N = 0.25$). This implies that the sparser the SCF (the compression ratio can be small), the probability of having a full-column rank matrix

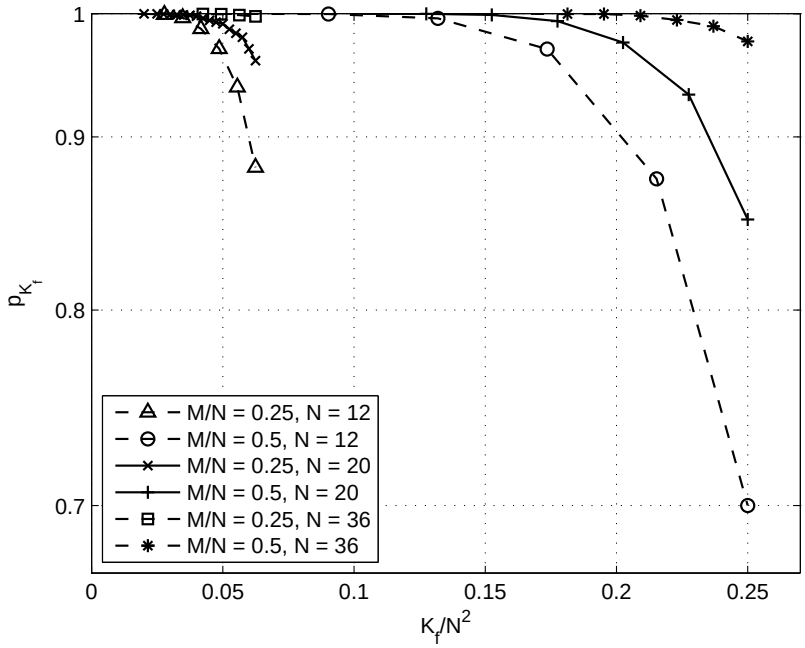

Figure 2: Probability that every K_f columns of $\tilde{\mathbf{\Phi}}$ forms a full-column rank $\hat{\mathbf{\Phi}}$, where $Spark(\tilde{\mathbf{\Phi}}) \leq K_f \leq Rank(\tilde{\mathbf{\Phi}})$ for $M/N = 0.25$ and $M/N = 0.5$ for increasing values of N.

is higher, yielding a unique solution with a higher probability. Secondly, at a given compression ratio, operating at higher values of N increases the probability of choosing a subset of K_f independent columns substantially. This results in an inherent trade-off between the reconstruction complexity which is directly proportional to M^2 and N^2 and the probability that the solution to the reconstruction will be unique. Finally, we can conclude that the *Spark* only gives a worst-case condition for the existence of a unique solution. In general, we can do better as is evident from the plot where even for moderate values of N ($N = 36$), the probability p_{K_f} is greater than 0.98.

The previous experiment inherently assumes that we are operating in a high SNR region and thus we do not always reconstruct the N PSD points of the SCF. But in a low SNR regime, the noise power is high and the PSD points always have high values. It is therefore imperative to reconstruct the PSD when operating at low SNRs. In order to meet this condition, we add a constraint to the way we choose the K_f columns from the $\tilde{\mathbf{\Phi}}$ matrix, i.e. instead of randomly selecting any set of columns, we ensure that the N PSD columns are always a subset

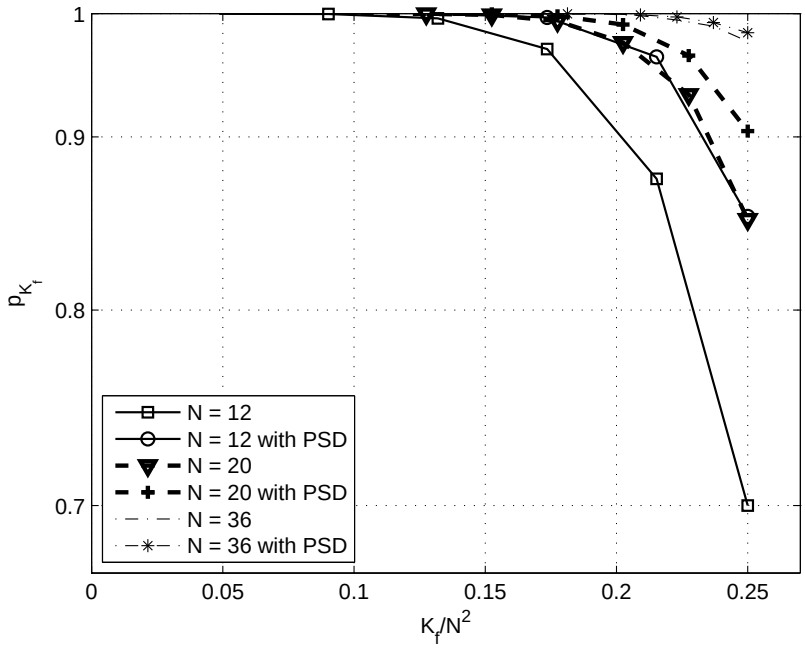

Figure 3: Probability that every K_f columns of $\tilde{\mathbf{\Phi}}$ forms a full-column rank $\hat{\mathbf{\Phi}}$, where $N \leq K_f \leq Rank(\tilde{\mathbf{\Phi}})$ for $M/N = 0.5$ for increasing vaues of N. The columns corresponding to PSD are always present in every subset.

of the K_f columns. Hence, now K_f is in the range $N \leq K_f \leq M^2$ which is a special case of $M+1 \leq K_f \leq M^2$ since $M < N$.

Fig. 3 compares the probabilitiy p_{K_f} when $M+1 \leq K_f \leq M^2$ to the special case that the N PSD columns are always a subset of the K_f columns ($N \leq K_f \leq M^2$). Similar to the previous experiment, we vary M and N for a fixed compression ratio $M/N = 0.5$. From the plot, we conclude that the probability of K_f columns being independent is higher when the N PSD columns are always selected as compared to a complete random selection of columns. Since this result corresponds to low SNRs, the increase in p_{K_f} is very beneficial as we are most interested in operating in a low SNR regime. Hence with higher probabilty a subset of K_f columns will be independent yielding a unique solution to the reconstruction. Furthermore, it is evident that the improvement with respect to p_{K_f} gradually diminishes as we go higher in N. Hence, the performance gap between varying values of N shrinks which increases the possibility of existence of a unqiue solution using a low-complexity reconstruction.

In light of the results above and in section 4.1 about the *Spark* of the measuement matrix $\tilde{\mathbf{\Phi}}$, we now formally state the conditions which guarantee a unique solution to the reconstruction problem.

4.3 Condition for Uniqueness of the Reconstructed Nyquist SCF $\hat{\mathbf{s}}_x$

The least-squares problem given in (13) can be solved if the system of equations is overdetermined, i.e, if $M^2 \geq K_f$. However, we have proven above that a unique solution to the reconstruction problem exists with probability 1 if $M + 1 > K_f$. In addition, we have shown that if $(M + 1) \leq K_f \leq M^2$, then a unique solution exists with a very high probability p_{K_f}. Thus, the solution to the least-squares problem always exists and is unique, resulting in the following theorem.

Theorem 2. *Let the system of equations,* $\mathbf{s}_z = \hat{\mathbf{\Phi}}\hat{\mathbf{s}}_x$ *be overdetermined with* $M^2 \geq K_f$*. The solution to the reconstruction of the cyclic features of the vectorized Nyquist SCF always exists and is unique with probability 1 iff* $K_f \leq M$*, or with probability* p_{K_f} *iff* $M + 1 \leq K_f \leq M^2$*, and is given by*

$$\hat{\mathbf{s}}_x = \hat{\mathbf{\Phi}}^{\dagger}\mathbf{s}_z = [\hat{\mathbf{\Phi}}^H\hat{\mathbf{\Phi}}]^{-1}\hat{\mathbf{\Phi}}^H\mathbf{s}_z. \tag{17}$$

In the next section, we relate the conditions for uniqueness of the reconstruction given by (17) to the compression ratio and the sparsity of the wideband channel.

5 Minimum Lossless Sampling Rates and Channel Sparsity

In accordance with the compressive sampling literature, we can sample below the Nyquist rate given that the signal is sparse in a particular domain. In order to ensure lossless reconstruction of the signal, there are limits on the minimum sampling rates which is governed by the sparsity in the signal. By exploiting sparsity in the PSD, the minimum compression ratio for a non-blind reconstruction (*Landau rate*) can be as low as the spectrum occupancy [27], defined as the ratio between occupied bandwidth to the total channel bandwidth. Using tunable oscillators or

parallel narrowband receivers, the *Landau rate* can be acheived at any SNR level and is given by

$$\left(\frac{M}{N}\right)_{Landau} = \frac{K_{f,PSD}}{N} = 2K\frac{B}{f_{nyq}}. \tag{18}$$

However, with a wideband receiver utilizing a single non-tunable RF chain, the PSD sparsity can only be exploited if we are operating in a high SNR region. At low SNRs, as the noise power is high, the PSD is not sparse any more and hence we cannot reduce sampling rates using only PSD sparsity. By operating in the cyclic domain, the sparsity has to account for non-zero cyclic frequencies as well, which yields a sparser transformation domain, and intuitively, the compression ratio can be reduced further. Since the noise is stationary, there are no features at non-zero cyclic frequencies which enables us to reduce sampling rates even at low SNRs.

We now derive bounds for the minimum lossless sampling rates achievable based on the sparsity/cardinality (K_f) of the SCF given in (16) using the uniqueness conditions dervied in section 4. From Theorem 2, we obtain a unique solution to the Nyquist SCF reconstruction with probability 1 iff $M \geq K_f$, or with probability p_{K_f} iff $M+1 \leq K_f \leq M^2$. For the case, $M \geq K_f$, the minmum sampling ratio is given by $(\frac{M}{N})_{\min} = \frac{K_f}{N}$. From (11) and (12), we have that $K_f \sim N^2$ and thus $\frac{K_f}{N} \sim N$. Hence, with increasing N (increasing resolution in f and α) the minimum sampling ratio becomes greater than 1. This is because in typical sensing problems the condition $M \geq K_f$ is violated as the number of non-zero points K_f in the SCF is greater than M and therefore no meaningful bound on minimum sampling rates can be derived.

We now focus on the range $M+1 \leq K_f \leq M^2$ which guarantees a unique solution with probability p_{K_f}. From section IV-B, we see that the probability p_{K_f} is a function of compression ratio and N. To obtain a lower bound on the minimum sampling rate we study the case when $K_f = M^2$ which is achieved wih probability p_{M^2}. This choice of K_f is not unrealistic as is shown in section IV-B where for moderate M and N ($M = 18, N = 36$), p_{M^2} is greater than 0.98. Thus the lower bound is given by

$$\begin{aligned}\left(\frac{M}{N}\right)_{cyclic} &= \sqrt{\frac{K_f}{N^2}} \\ &= \begin{cases} 2\sqrt{K}\frac{B}{f_{nyq}} & \text{under high SNR} \\ \sqrt{\frac{4KB^2}{f_{nyq}^2} + \frac{1}{N} - \frac{2KB}{N^2 f_{nyq}}} & \text{under low SNR} \end{cases}\end{aligned} \tag{19}$$

In (19), as $N \to \infty$, for low SNR $(\frac{M}{N})_{cyclic} \to 2\sqrt{K}\frac{B}{f_{nyq}}$ which is same as the result for high SNR. This is intuitive because as $N \to \infty$, the ratio $\frac{N}{N^2} \to 0$ and therefore the number of PSD points are negligible compared to the area of the SCF. Thus asymptotically the minimum lossless sampling ratio is independent of SNR.

The minimum sampling rate for $K_f = M(M+1)/2$ under a high SNR regime can similarly be expressed as

$$\left(\frac{M}{N}\right)_{cyclic} = \frac{-1 + \sqrt{1 + \frac{32KN^2B^2}{f_{nyq}^2}}}{2N}. \tag{20}$$

From the expressions for minimum achievable sampling ratios in (18) and (19) corresponding to energy and cyclostationary detection respectively, it is evident that cyclostationary detectors require lower sampling rates for the same PSD sparsity levels. As this difference in minimum sampling ratios is $\sim \sqrt{K}$, where $K > 1$, with increasing number of signals in the band/decreasing sparsity, cyclostationary detectors have correspondingly increasing gains compared to energy detectors.

6 Discussion And Numerical Results

In order to detect the presence/absence of the primary users using our proposed algorithm, we consider a wideband channel of bandwidth 300 MHz, occupied with K BPSK signals, one of which is the signal of interest (SOI). Each of the K signals has an effective signal bandwidth of 15 MHz (taking into account the roll-off factor of the pulse-shaping filter). As mentioned earlier, the noise is assumed to be AWGN with an equal in-band SNR for all signals, and a frame length $N = 36$ samples. The spectral correlation peak considered for single-cycle detection is at $(\alpha, f) = (2f_c, 0)$.

The detection performance of the reduced-complexity detector is evaluated by reconstructing only K_f points in the SCF. However, the number of reconstructed spectral correlation peaks is greater than that given by (12). This is because, at $N = 36$, the frequency resolution in f and α is not sufficient to see all the features of the active signals which results in spectral leakage into the adjacent bins. This leakage results in more non-zero points in the SCF which we need

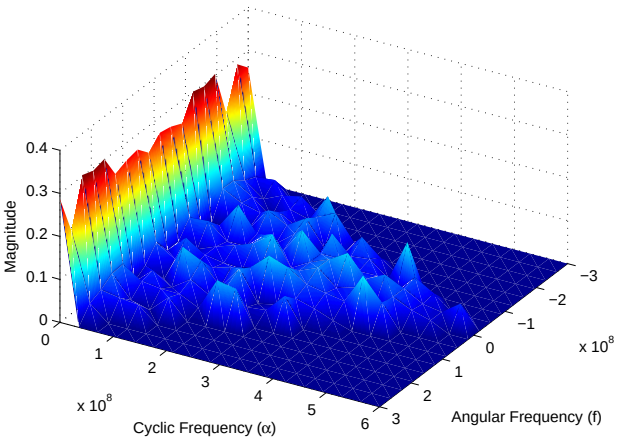

(a) Sub-Nyquist SCF $\mathbf{s}_z$ obtained from the autocorrelation $\mathbf{r}_z$.

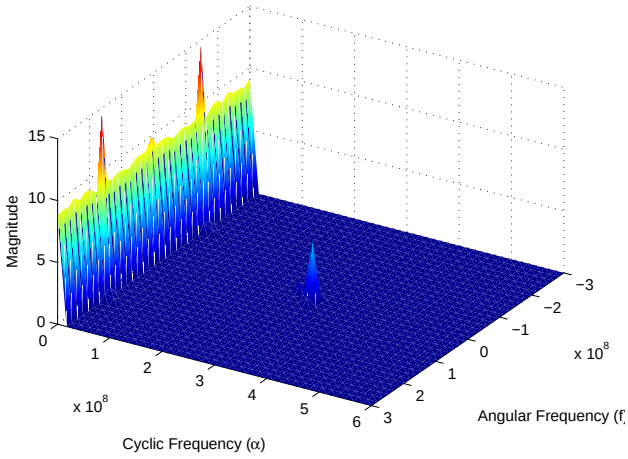

(b) Reconstructed Nyquist SCF $\hat{\mathbf{s}}_x$ using the relation $\mathbf{s}_z = \hat{\mathbf{\Phi}}\hat{\mathbf{s}}_x$.

Figure 4: Comparison of sub-Nyquist and Reconstructed SCFs at a compression ratio $M/N = 0.5$, L = 2000 averages and SNR = 0 dB.

to reconstruct.

The rest of this section is organized as follows. In Section 6.1, we demonstrate the working of the proposed reconstruction algorithm. Section 6.2 compares the theoretical minimum compression ratios of the proposed cyclostationary-based detector to that of an energy detector. In Section 6.3, we evaluate the mean-squared error of the reconstruction for various compression ratios. Section 6.4 shows the relationship between the required sensing time and SNR to reach a desired point on the ROC curve. Finally, Section 6.5 shows the effect of the sensing time, compression ratio, and SNR on the detection performance.

6.1 SCF Reconstruction Using the Proposed Algorithm

In this section, we demonstrate how the Nyquist SCF is reconstructed from the sub-Nyquist samples for a BPSK signal. The sub-Nyquist samples are acquired at a compression ratio $M/N = 0.5$, SNR = 0dB. In order to compute the sub-Nyquist SCF $\mathbf{s}_z$ shown in Fig. 0.4(a), we first obtain the autocorrelation matrix $\mathbf{r}_z$ using $L = 2000$ frame averages of the sub-Nyquist samples

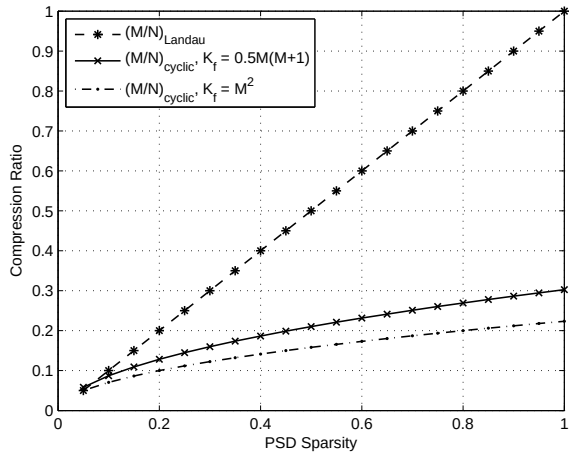

(a) Minimum Sampling Rates for Energy detection vs. Cyclostationary Detection at High SNRs

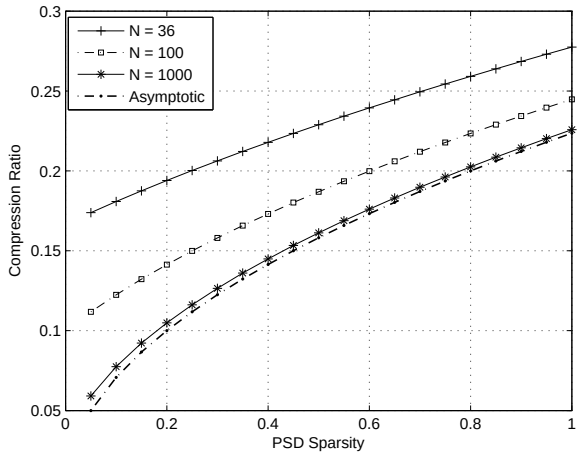

(b) Minimum Sampling Rates for Cyclostationary Detection, for $K_f = M^2$ at Low SNRs for increasing values of N.

Figure 5: Minimum Sampling rate vs PSD Sparsity

$\mathbf{z}$ and then take double Fourier transform with respect to (t, τ). We can see that the sub-Nyquist SCF has no spectral correlation peaks. This is because, when the random i.i.d Gaussian matrix $\mathbf{A}$ multiplies the correlated elements of $\mathbf{x}$, the resulting vector $\mathbf{z}$ loses its spectral correlation and therefore its SCF looks like one of a stationary process.

Fig. 0.4(b) shows the reconstructed Nyquist SCF which we obtain using Eq. (14). The PSD and the peak at $(2f_c, 0)$ confirms that the reduced complexity reconstruction algorithm works well. Note that we only reconstruct K_f points in the SCF which correspond to the PSD and the expected BPSK peaks as given in Table 1. Further, the resolution in f and α is not high enough at low N and hence we not see the peaks at $(2f_c \pm \frac{1}{T}, 0)$ and $(\frac{1}{T}, f_c)$.

6.2 Theoretical Minimum Lossless Compression

Here, we compare the minimum lossless sampling rates for energy detectors given by the Landau rate in (18) and the lower bounds on sampling rates for Cyclostationary detectors corresponding to $K_f = M^2$ and $M(M+1)/2$ in (19) and (20). From Fig. 0.5(a), we observe that at high SNRs, when the channel is completely populated with signals, by exploiting the sparsity in the cyclic

domain α, we can achieve significantly lower sampling rates. We can go as low as $M/N = 0.23$ for $K_f = M^2$, giving about 80% lower sampling rates and for $K_f = M(M+1)/2$, we gain about 70% compared to the Landau rate.

In Fig. 0.5(b), we study the minimum acheivable sampling rates at low SNRs. In this scenario, with only PSD sparsity, we cannot go lower than the Nyquist rate irrespective of the actual number of signals present in the band of interest but we can exploit the sparsity in the cyclic frequency domain (α) to go lower than the Nyquist rate. The plot in Fig. 0.5(b) shows the lower bounds on the minimum lossless sampling rates for $K_f = M^2$ for increasing values of N. From the results, we conclude that, with increasing N, the minimum sampling rates for cyclostationary detectors converges to the rates achievable at high SNRs, the lower bound on the sampling rates. However, for moderate values of N, for instance $N = 36$, we need about 10% higher sampling rates compared to the lower bound. Hence, there exists a tradeoff between the analog sampling rates and digital processing required for reconstruction. A higher sampling rate analog front-end reduces the energy spent in DSP, whereas sampling close to the lower bound on the analog front-end requires high computational power for reconstruction due to the requirement of a very high value for N to reduce sampling rates.

6.3 Mean Squared Error (MSE) of the Reconstructed SCF

In this section, we compute the mean-squared error of the reconstructed spectral correlation peak $(2f_c, 0)$ used for detection with respect to its energy under no compression (Nyquist) denoted by s_{x_i}. The MSE is defined as

$$\text{MSE} = \mathbb{E}\left[|\hat{s}_{x_i} - s_{x_i}|^2/|s_{x_i}|^2\right]$$

where $\hat{s}_{x_i}$ is the cyclic feature used for detection. As we consider only finite number of samples to compute the autocorrelation, the number of frame averges L used is large (of the order of 1×10^4) to smoothen out the noise fluctuations. We consider noiseless signals, all of the same energy and compute the MSE for decreasing compression ratios M/N. Fig. 6 shows the MSE versus compression ratio curve for the channel populated with $K = 1$ and 3 signals, yielding a PSD occupancy of 5% and 15% respectively.

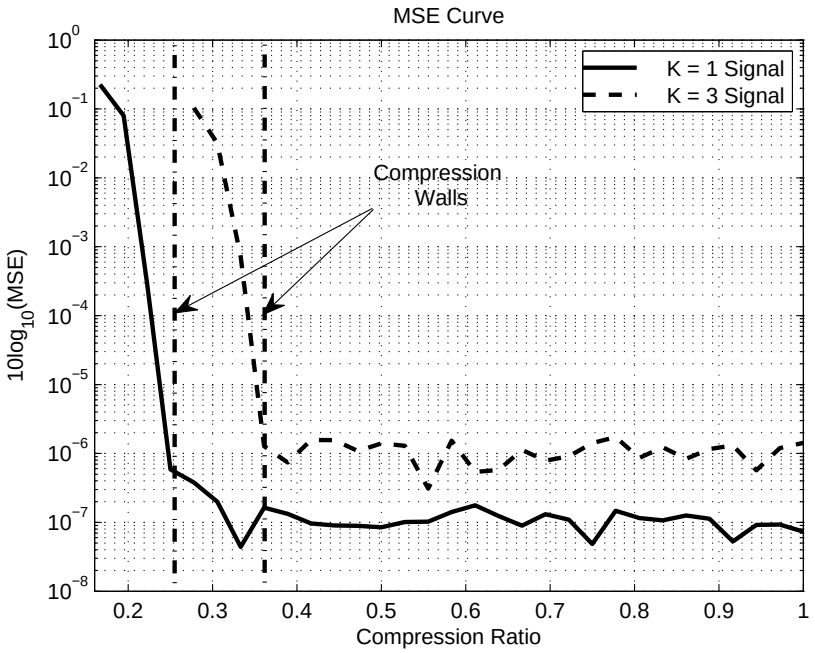

Figure 6: Minimum Squared Error(MSE) of Reconstructed Feature used for Signal Detection under Varying Sparsity Levels, $K = 1$ and $K = 3$ Signals.

The MSE curves show that up to a certain threshold compression ratio there is no loss in energy and the signal reconstruction is perfect. Below this threshold compression ratio, the MSE increases exponentially with decreasing compression ratio. This is because, below this point the reconstruction problem in (13) is under-determined and hence the signal reconstruction fails. Therefore, when $\hat{\mathbf{s}}_x$ is truly sparse (with sufficient L), the sampling rate can be reduced up to a certain threshold with no loss incurred, a point that we refer to as *compression wall*. The vertical lines in Fig. 6 point to the location of the *compression walls* for different PSD occupancies. Note that the minimum lossless compression ratios obtained numerically in Fig. 6 are higher than the theoretical bounds computed using Eq. (19) due to spectral leakage of the signal at low N, which results in more non-zero features that we need to reconstruct.

6.4 Sensing Time Requirements and Comparison to Nyquist Detection

In this section, we quantify the additional sensing time required to reach $(P_{fa}, P_d) = (0.1, 0.9)$ at various SNRs/compression ratios using our reduced-complexity detector.

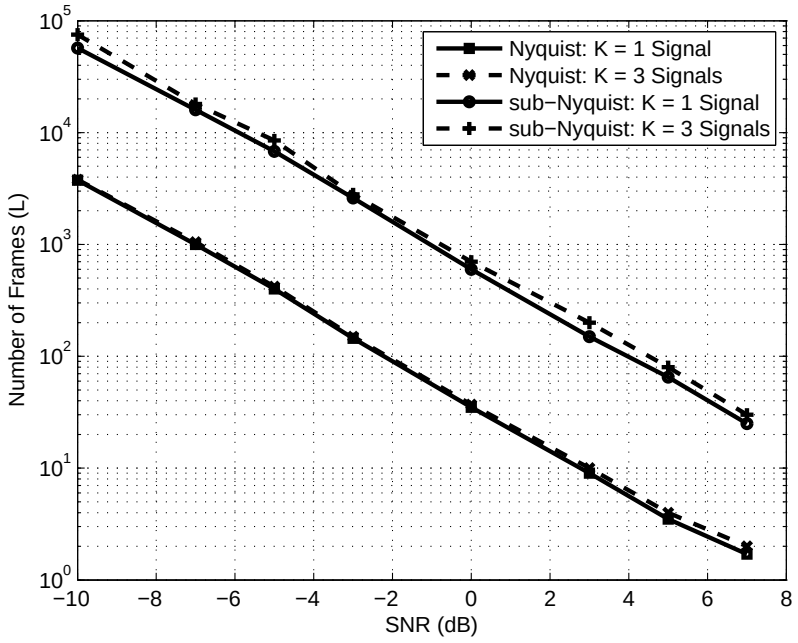

Figure 7: Number of frames(L) required to reach $(P_{fa}, P_d) = (0.1, 0.9)$ versus SNR for Nyquist and sub-Nyquist based detectors for a Compression Ratio of $M/N = 0.5$, with $K = 1$ and 3 Signals.

We start by empirically finding the relationship between the sensing time (number of frames L) and SNR for cyclostationary-based sub-Nyquist detectors at a compression ratio $M/N = 0.5$. We then compare this to Nyquist-based detectors for varying PSD sparsity levels (5% and 15%) as shown in Fig. 7. The results show that the for sub-Nyquist based detection, the sensing time increases linearly (in dB scale) with decreasing SNR and the slope of the curve is equal to that of the Nyquist detector. Hence, the reconstruction using our algorithm conserves the linear relationship(in dB scale) between SNR and sensing time for cyclostationary detectors. Further, increasing the number of active signals in the PSD does not require a huge amount of increase in the sensing time.

Fig. 8 shows the trend of total number of samples/sensing time($L \times M$) required to reach $(P_{fa}, P_d) = (0.1, 0.9)$ with decreasing compression ratio. This is evaluated at SNR $= -5$ dB for a channel occupied with $K = 1$ and 3 signals. As can be seen from the plot, with decreasing compression ratio, there is a steady increase in the required sensing time upto the compression

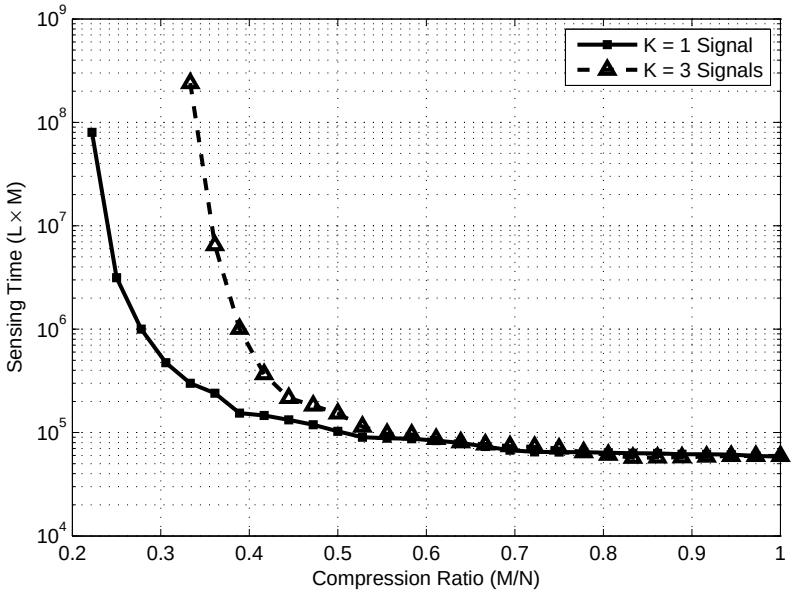

Figure 8: Sensing Time versus Compression Ratio to reach $(P_{fa}, P_d) = (0.1, 0.9)$ for Varying Sparsity Levels, $K = 1$ and 3 Signals and SNR = -5 dB.

wall (0.3 for 5% sparsity and 0.4 for 15% sparsity). However, operating at a compression ratio below the compression wall requires an exponentially increasing number of samples in order to operate at the same point on the ROC, which makes the detection infeasible within a constrained sensing time. This explains the tradeoff between the sensing time and reduction in sampling rates, where being close to the compression wall is the optimum point to be at since the maximum savings in terms of sampling rates can be achieved with only a linear increase in sensing time.

6.5 Detection Performance of the Proposed Detector

In this section we analyze the detection performance of the proposed algorithm for varying parameters. Firstly, we show the effect of varying the compression ratio under a fixed SNR $= -10$dB and $L = 15000$ averages for a fixed sparsity of 15% ($K = 3$ signals). Fig. 9 shows that with decreasing sampling rates, there is a gradual decay in detection performance. The decay in performance is mainly due to the presence of the undesired spectral correlation peaks of noise in the SCF which we do not reconstruct. This implies that $L = 15000$ averages are not enough to

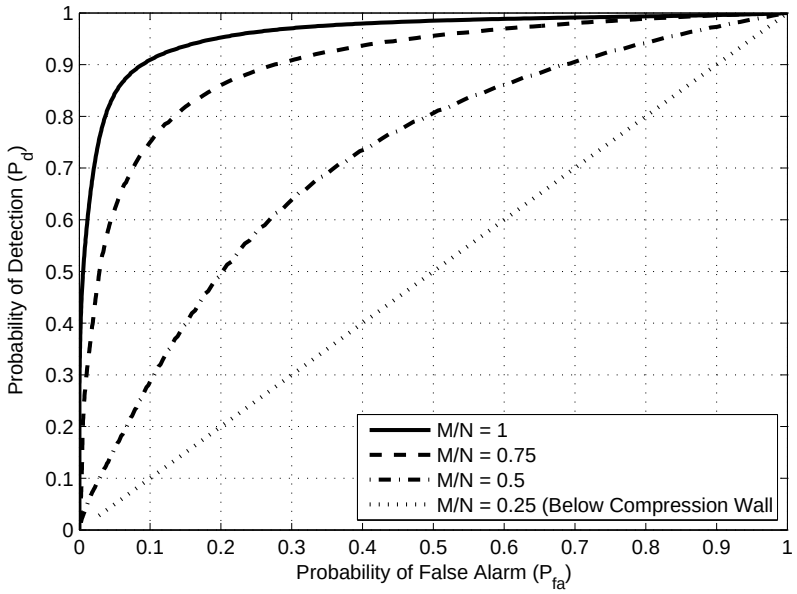

Figure 9: P_d versus P_{fa} for Varying Compression Ratio($\frac{M}{N}$) for $K = 3$ Signals, Number of Frame Averages L = 15000 and SNR = -10 dB.

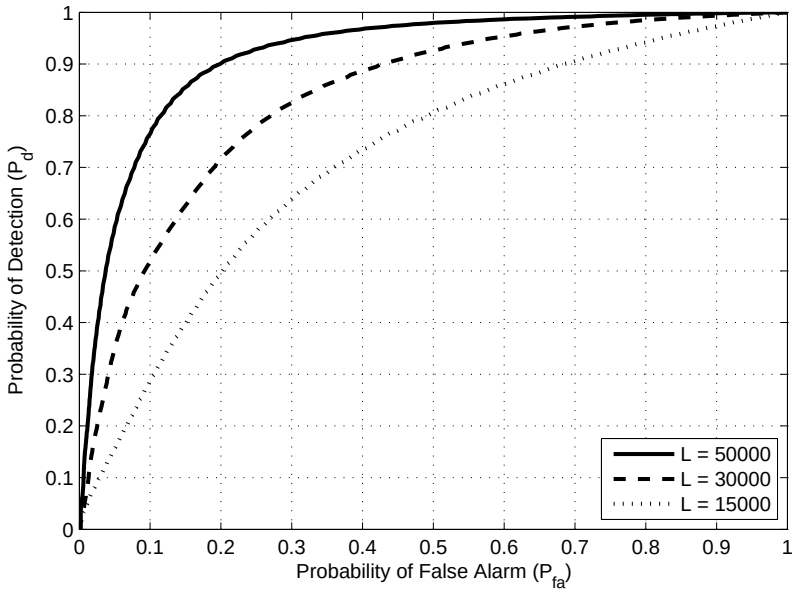

Figure 10: P_d versus P_{fa} for Varying Frame Averages for $K = 3$ Signals, Compression Ratio M/N = 0.5 and SNR = -10 dB.

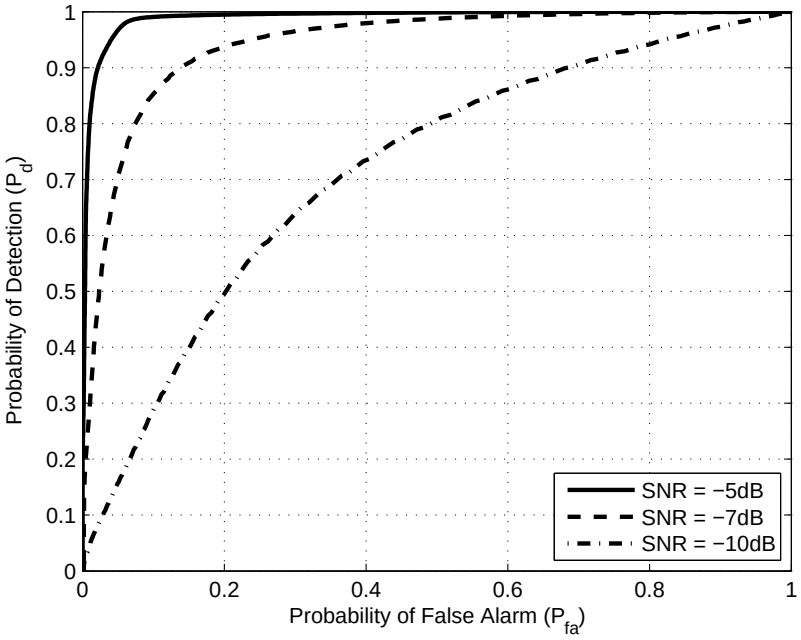

Figure 11: P_d versus P_{fa} for Varying SNR for $K = 3$ Signals, Compression Ratio M/N = 0.5 and Number of Frame Averages L = 15000.

ensure that the reconstructed $\hat{\mathbf{s}}_x$ is truly sparse. Under enough averages, the peaks due to noise are smoothened out, and therefore the ROC curves will match with increasing L. The detection performance below the compression wall worsens drastically giving a linear relationship between P_d and P_{fa}.

The presence of unwanted spectral correlation peaks at low SNRs in the reconstructed SCF can be compensated by increasing the number of frame averages L. Fig. 10 shows the improvement in detection performance with increasing number of averages for fixed SNR $= -10$dB, compression ratio $M/N = 0.5$ and $K = 3$ signals. The detection performance improves with increasing L as this corresponds to additional sensing time and also as the sparsity of the reconstructed SCF converges to its true sparsity.

Finally, we show the impact of varying SNR on detection performance for fixed $L = 15000$, compression ratio $M/N = 0.5$ and $K = 3$ signals. From Fig. 11 we can see that the detection performance improves with increasing SNR as 1) the signal power increases and 2) with increasing SNR the reconstructed SCF approaches its true sparsity. In fact, increasing SNR is equivalent

to increasing the number of samples used for averaging the SCF, and the trend is similar to the ROC curves presented in Fig. 10.

r

7 A Practical Example: Modulated Wideband Converter (MWC)

In our work thus far, we have considered a random i.i.d Gussian matrix $\mathbf{A}$ to model the analog front-end used to acquire the sub-Nyquist samples $\mathbf{z}$. In this section, we take a more practical approach and analyze the performance of the cyclostationary-based sub-Nyquist detector using the Modulated Wideband Converter [9–11] as the sampling front-end. The rest of the section is organized as follows. In section 7.1, we introduce the MWC and establish the relationship between the Nyquist and sub-Nyquist samples. In Section 7.2, we recover the Nyquist samples and compute the Nyquist SCF. Finally, Section 7.3 gives the numerical results.

7.1 System Overview

The MWC consists of an analog-front end with m parallel channels. In each channel, the input signal $x(t)$ is multiplied by a periodic waveform $p_i(t)$, low-pass filtered and then sampled at a rate $B_k = 1/T$, where B_k is the bandwidth of each signal k in $x(t)$, for $k \in [1, ..., K]$. Here, we assume that the sampling interval T equals the period of the waveform $p_i(t)$.

The main idea behind the MWC is the mixing operation performed by the periodic waveform $p_i(t)$ which scrambles the spectrum of $x(t)$ such that the baseband frequencies contain a mixture of spectral contents from the entire Nyquist range. This is due to aliasing of frequencies spaced $1/T$ apart at baseband. Now, since $p_i(t)$ is periodic, we can model an equivalent simplified form of the MWC using which we obtain a relationship between the Nyquist and sub-Nyquist samples.

Consider the Nyquist bandwidth B which is divided equally into Q bands ($m \ll Q$). Then the MWC can be conceptually thought of as a front-end with Q parallel branches, where in each branch, one band of the input signal $x(t)$ is downconverted to baseband, low-pass filtered and then sampled at a rate $1/T$. Hence, at the output of the Q branches we have for each time-point

the vector $\mathbf{v}[n] = [v_{-L}[n], ..., v_L[n]]^T$. Since the signal $x(t)$ is sparse, most of the Q bands are empty and hence $\mathbf{v}[n]$ can be compressed into the output $\mathbf{y}[n] = [y_1[n], ..., y_m[n]]^T$ using the linear projection

$$\mathbf{y}[n] = \mathbf{C}\mathbf{v}[n] \tag{21}$$

where $Q = 2L+1$, the Nyquist baseband samples $\mathbf{v}[n] \in \mathbb{R}^Q$, the sub-Nyquist samples $\mathbf{y}[n] \in \mathbb{R}^m$ and the projection matrix $\mathbf{C} \in \mathbb{R}^{m \times Q}$. To develop the equivalence of the MWC to the simplified model, we use the fact that as $p_i(t)$ is T-periodic, it has a Fourier series expansion

$$p_i(t) = \sum_{l=-\infty}^{\infty} c_{il} e^{j\frac{2\pi}{T}lt}$$

Choosing the matrix $\mathbf{C}$ in (21) such that its ilth entry is equal to the Fourier coefficient c_{il} results in the equivalence of the MWC to this simplified model [11]. Given that we have a relation between the Nyquist and sub-Nyquist samples in (21), in the next section, we compute the Nyquist SCF from the reconstructed Nyquist samples which is then used for signal detection.

7.2 Recovery of Nyquist Samples

The goal of the reconstruction scheme is to recover the baseband Nyquist samples $\mathbf{v}[n]$ from the samples $\mathbf{y}[n]$. From Eq. (21), as $m \ll Q$, in order to solve for $\mathbf{v}[n]$, we need to find the support $\mathcal{S}$ of the signal $\mathbf{v}[n]$. Once the support $\mathcal{S}$ is known, reconstructing $\mathbf{v}[n]$ is possible if the submatrix $\mathbf{C}_\mathcal{S}$, which contains the columns of $\mathbf{C}$ indexed by $\mathcal{S}$, has full-column rank. In this scenario,

$$\hat{\mathbf{v}}_\mathcal{S}[n] = \mathbf{C}_\mathcal{S}^\dagger \mathbf{y}[n] \tag{22}$$

where $\hat{\mathbf{v}}_\mathcal{S}[n]$ is the reconstructed signal vector which has entries corresponding to the support $\mathcal{S}$ of $\mathbf{v}[n]$. Given the *a priori* knowledge about the signal parameters, namely the modulation class, the carrier frequency, and the symbol rate of the PU that we wish to detect, here we consider a non-blind detection scenario and therefore the support $\mathcal{S}$ is assumed to be known.

Given that we have the reconstructed baseband time-domain Nyquist samples $\hat{\mathbf{v}}_\mathcal{S}[n]$ from (22), we can recover our original signal $x(t)$ by interpolating $\hat{\mathbf{v}}_\mathcal{S}[n]$ to the Nyquist rate and finally upconverting and summing the interpolated sequences together. The Nyquist SCF can then be computed using Eq. (2) which is used for signal detection.

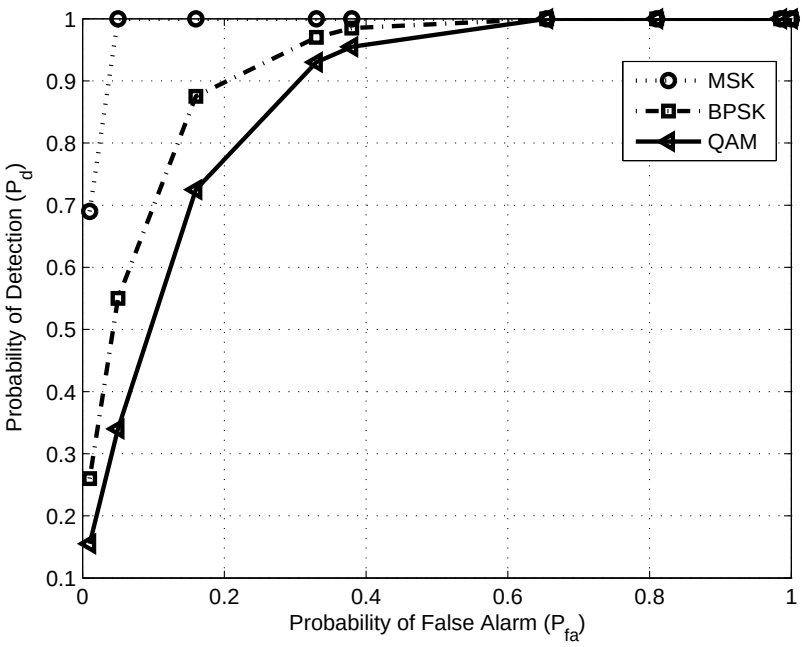

Figure 12: P_d versus P_{fa} for different modulation classes at $L = 100$ frame averages and SNR = 0 dB.

7.3 Numerical Results

In this section, we show the performance of the proposed detector using the MWC analog front-end. We consider a wideband channel of bandwidth 10 GHz with $K = 4$ transmitters that are possibly active. Each of the active signals has a maximal bandwidth of $B_k = 2$ MHz. The analog front-end consists of $m = 10$ parallel hardware channels and the sampling rate of each channel is $f_s = B_k = 2$ MHz. Further, the waveform $p_i(t)$ is chosen as a piecewise constant function that alternates between ± 1 at the Nyquist rate for a period $T = 1/B_k$. Formally.

$$p_i(t) = \alpha_{ik}, \quad with \;\; \alpha_{ik} \in \{+1, -1\}$$

and $p_i(t + nT) = p_i(t)$ for every $n \in \mathcal{Z}$. On the digital side, we collect $L = 100$ frames of $N = 1024$ samples each that are used for averaging of the SCF.

Fig. 12 shows the ROC curves resulting from the cyclostationary detection for three different modulation classes at SNR = 0dB. The effective sampling rate of the analog-front end is $mf_s = 20\text{MHz} \ll B$. From the curves we observe tha MSK has the best detection performance followed

by BPSK and 4-QAM. This is because of the strength and number of features of the respective modulation classes as can be seen in Table 1.

8 Conclusion

We have presented in this thesis a compressive sampling approach for wideband spectrum sensing which directly reconstructs the test statistic used for cyclostationary detection. The detection performance of the reduced-complexity solution which only reconstructs spectral features in the asymptotic SCF of the signal of interest suffers from a loss with respect to the full reconstruction whenever the sensing time is not sufficient to make the SCF truly sparse. With increasing sensing time, the sparsity of the SCF reaches its asymptotic value by averaging the noise, the point at which the reduced complexity detection matches that of the full reconstruction. The theoretical lossless compression wall has been derived for a given spectral correlation function sparsity, which is a function of bandwidth, modulation class, and number of PU signals in a given band. By comparing the minimum achievable lossless compression ratios of both cyclostationary and energy detectors for a given sparsity level, it has been shown that the additional sampling rate savings in the feature-based detection are possible due to the higher degree sparsity in cyclic domain than in frequency domain alone. We have shown that in order to operate at the required point on the ROC, there is slight increase in sensing time compared to Nyquist sampling when the compression ratio is above the compression wall. However, operating below the compression wall requires an exponentially increasing sensing time.

References

[1] D. Cabric, S. Mishra, and R. Brodersen, "Implementation issues in spectrum sensing for cognitive radios," in *Asilomar Conference on Signals, Systems and Computers*, 2004.

[2] T. Yucek and H. Arslan, "A survey of spectrum sensing algorithms for cognitive radio applications," *Communications Surveys Tutorials, IEEE*, vol. 11, no. 1, pp. 116–130, Jan. 2009.

[3] A. Ghasemi and E. S. Sousa, "Spectrum sensing in cognitive radio networks: Requirements, challenges and design trade-offs," *IEEE Communications Magazine*, pp. 32–39, Apr. 2008.

[4] Y. Zeng, Y.-C. Liang, A. T. Hoang, and R. Zhang, "A review on spectrum sensing for cognitive radio: Challenges and solutions," *EURASIP Journal on Advances in Signal Processing*, pp. 1–15, Jan. 2010.

[5] W. Gardner, *Statistical spectral analysis: a non probabilistic theory.* Prentice Hall, 1988.

[6] A. Sahai and D. Cabric, "Spectrum sensing – fundamental limits and practical challenges," in *IEEE DySpan Conference*, Nov. 2005, Baltimore.

[7] D. Donoho, "Compressed sensing," *IEEE Trans. Inf. Theory*, vol. 52, no. 4, pp. 1289 – 1306, Apr 2006.

[8] J. Laska, S. Kirolos, M. Duarte, J. Laska, S. Kirolos, and M. Duarte, "Theory and implementation of an analog-to-information converter using random demodulation," in *IEEE ISCAS*, May 2007.

[9] M. Mishali and Y. C. Eldar, "From theory to practice: Sub-nyquist sampling of sparse wideband analog signals," *IEEE J. Sel. Topics Signal Process.*, vol. 4, no. 2, pp. 375–391, Apr. 2010.

[10] ——, "Wideband spectrum sensing at sub-nyquist rates," *IEEE Signal Process. Mag.*, vol. 28, no. 4, pp. 102–135, Jul. 2011.

[11] M. Mishali, Y. C. Eldar, O. Dounaevsky, and E. Shoshan, "Xampling: Analog to digital at sub-nyquist rates," *Circuits, Devices Systems, IET*, vol. 5, no. 1, pp. 8–20, Jan. 2011.

[12] D. Wieruch and V. Pohl, "A cognitive radio architecture based on sub-nyquist sampling," in *IEEE DySPAN*, 2011, Aachen, Germany.

[13] Z. Yu and S. Hoyos, "Compressive spectrum sensing front-ends for cognitive radios," in *IEEE International Conference on Systems, Man, and Cybernetics*, 2009.

[14] X. Chen, L. Zhao, and J. Li, "A modified spectrum sensing method for wideband cognitive radio based on compressive sensing," in *IEEE International Conference on Communications and Networking in China*, 2009.

[15] M. F. Duarte and Y. C. Eldar, "Structured compressed sensing: From theory to applications," *IEEE Trans. Signal Process.*, vol. 59, no. 9, pp. 4053–4085, Mar. 2011.

[16] Y. Polo, Y. Wang, A. Pandharipande, and G. Leus, "Compressive wide-band spectrum sensing," in *Proc. IEEE ICASSP*, 2009, Taipei, Taiwan.

[17] Y. Wang, Z. Tian, and C. Feng, "A two-step compressed spectrum sensing scheme for wideband cognitive radios," in *IEEE GLOBECOM 2010*.

[18] E. Like, V. Chakravarthy, and Z. Wu, "Reliable modulation classification at low SNR using spectral correlation," in *Consumer Communications and Networking Conference, 2007. CCNC 2007. 4th IEEE*, Jan. 2007.

[19] D. Cohen, E. Rebeiz, V. Jain, Y. C. Eldar, and D. Cabric, "Cyclostationary feature detection from sub-nyquist samples," in *Fourth International Workshop on Computational Advances in Multi-Sensor Adaptive Processing*, 2011.

[20] Z. Tian, "Cyclic feature based wideband spectrum sensing using compressive sampling," in *International Conference on Communications*, Jun. 2011.

[21] E. Rebeiz, V. Jain, and D. Cabric, "Cyclostationarity-based low complexity wideband spectrum sensing using compressive sampling," in *International Conference on Communications*, Jun. 2012, Ottawa, Canada.

[22] E. Candes and T. Tao, "Near-optimal signal recovery from random projections: Universal encoding strategies?" *IEEE Trans. Inf. Theory*, vol. 52, no. 12, pp. 5406 – 5425, Dec 2006.

[23] R. G. Baraniuk, M. A. Davenport, R. A. DeVore, and M. B. Wakin, "A simple proof of the restricted isometry property for random matrices," *Constructive Approximation*, Jan 2007.

[24] S. Jokar and V. Mehrmann, "Sparse solutions to underdetermined kronecker product systems," *Linear Algebra and its Applications*, vol. 431, no. 12, pp. 2437 – 2447, 2009.

[25] M. Duarte and R. Baraniuk, "Kronecker compressive sensing," *IEEE Trans. Image Process.*, vol. 21, no. 2, pp. 494 – 504, Feb. 2012.

[26] A. M. Tillmann and M. E. Pfetsch, "The computational complexity of the restricted isometry property, the nullspace property, and related concepts in compressed sensing," *ArXiv e-prints*, May 2012.

[27] H. Landau, "Necessary density conditions for sampling and interpolation of certain entire functions," *Acta Math*, vol. 117, pp. 37–52, Jul. 1967.